



# Simplified methodology for fatigue analysis of reinforced asphalt systems

Marko Orešković · Štepan Bohuš ·  
Amedeo Virgili · Francesco Canestrari 

Received: 7 July 2023 / Accepted: 17 January 2024  
© The Author(s) 2024

**Abstract** Fatigue analysis has an important role in evaluating the durability and performance of asphalt pavements, especially when novel or alternative materials are used. Numerous laboratory studies have investigated fatigue performance with the aim of estimating field behavior as accurately as feasible. Therefore, there are currently many different test methods and data analysis approaches that can be used. One of the most common laboratory test methods is the four-point bending beam (4PBB) test, which results are usually analyzed using the so-called traditional (where 50% reduction in initial stiffness is considered as failure criterion) or the energy ratio (ER) approach. However, outcomes from previous studies have shown that these approaches may not be appropriate and reliable if geogrids are used as a reinforcement. As a possible solution, this study proposes a new simplified flex point (SFP) approach that considers the flex point of the strain amplitude curve, measured during 4PBB fatigue tests, to calculate the number of cycles to

failure. These three approaches were applied to four double-layered asphalt sets: one unreinforced and three reinforced with geogrids of different strength (50 x 50, 100 x 100 and 100 x 200 kN/m). The impact of reinforcement on the fatigue life was evaluated by comparing the critical strain values ( $\epsilon_c$ ) of reinforced and unreinforced sets through the fatigue resistance improvement factor. The research findings showed that the use of geogrids improves fatigue life when the SFP and ER approaches are applied and that the traditional approach might not always be appropriate for assessing the fatigue resistance of reinforced asphalt mixtures.

**Keywords** Asphalt fatigue · Four-point bending beam · Reinforcement · Geogrid · Fatigue improvement

## 1 Introduction

The first use of textiles in roads dates back to 1926 when a heavy cotton fabric was placed below asphalt layers, which led to improved cracking resistance, decreased localized road failures and reduced raveling [1]. Since then, geosynthetics (fabrics, composites, membranes, grids, etc.) have been widely utilized for different purposes within road construction, namely: for separation, filtration, stiffening, drainage and reinforcement [2]. The use of geogrids for reinforcement of asphalt layers within pavement structure

---

M. Orešković  
University of Belgrade, Faculty of Civil Engineering,  
Bulevar kralja Aleksandra 73, 11000 Belgrade, Serbia

Š. Bohuš  
Saint-Gobain ADFORS CZ s.r.o., Sokolovská 106,  
570 01 Litomyšl, Czech Republic

A. Virgili · F. Canestrari (✉)  
Università Politecnica Delle Marche, Via Breccie Bianche,  
60131 Ancona, Italy  
e-mail: f.canestrari@staff.univpm.it



is likely the most recent application of geosynthetics that started since the early 1980s, when geogrids were used to mitigate reflective cracking and to prolong fatigue life [3]. After then, numerous investigations involving geosynthetics have been carried out, concluding that they can successfully slow down reflective cracking propagation [4, 5] and improve fatigue [6–9] or rutting resistance [10, 11], even though they may affect shear bond strength [10, 12]. Research studies have been predominantly performed in laboratory conditions using small-scale tests because of their simplicity and low costs [3, 8, 10, 13–16] or medium-scale tests [17, 18], whereas other studies [12, 19–22] carried out in-situ tests which may give more reliable results. The beneficial effects of geogrids on the pavement structure have also been assessed through the life cycle cost analysis (LCCA) [10]. The results showed that sections reinforced with geogrids can significantly reduce maintenance and construction costs during a 20-year service period when compared to the section without reinforcement. In another study, it was claimed that a grid reinforcement has a potential to structurally reduce the required thickness of the asphalt layers [23]. Overall, it can be concluded that the application of geogrids may affect the durability of pavement structures, so certain studies have modified existing pavement design methods considering the presence of geogrids [21, 22, 24].

There are several types of geogrids used for pavement reinforcement, where some of them are woven from glass fibers of polymeric filaments, whereas others can be cut or pressed from plastic sheets and then post-tensioned to maximize strength and modulus [25]. Grids typically have squared, hexagonal or rectangular mesh shapes, with openings from 6 to 50 mm, whose ribs can be made of materials with different strength in two perpendicular directions. Fiberglass yarns used for the production of geogrids can be coated with bitumen-based or polymer-based coating (to protect them and to reach an effective bonding between asphalt layers). As an interlayer system, reinforcement can be in the form of geogrid or it can also contain a layer of light or heavy non-woven fabric. It can be placed at different positions and depths within a pavement structure—below or between asphalt layers with aim to reduce permanent deformation and differential settlement or to mitigate reflective or fatigue cracking [3]. A reinforcement is usually located at

the interface of two asphalt layers or between asphalt concrete overlay and a concrete pavement. Because the presence of such reinforcement can weaken the interlayer bond, numerous studies have proposed applying a larger tack coat content than usual to compensate for the otherwise observed reduction in bonding quality, even when using self-adhesive grids [17, 26]. This is supposed to ensure a good interlayer bond as it has been demonstrated that interlayer fatigue failure usually occurs due to improper tack coat content and inadequate construction practices [27].

In recent years, many studies have been conducted to evaluate the impact of geogrids on pavement performance. Among the frequently utilized laboratory tests are: three point bending beam—3PBB [12, 28, 29], four point bending beam—4PBB [6, 9, 14, 30], ASTRA interface direct shear test [12, 14] and overlay tester—OT [5, 31]. The fact that some researchers had designed different types of testing configurations such as the shear-torque fatigue test [18] and anti-reflective cracking system [4, 32, 33] further illustrates how crucial it is to examine the impact of grid reinforcement on pavement performance. However, due to the convenience of preparing specimens with geogrids, 3PBB and 4PBB tests have been widely employed in earlier investigations.

To better understand the mechanism of reinforcement in pavement structure and to examine its impact on fatigue performance, a variety of test specimens for the 3PBB and 4PBB tests have been investigated in previous studies. The geogrid location has varied in these studies as it has been demonstrated that their location has a substantial impact on the fatigue life [34, 35]. Only a small number of studies [30, 36] have been conducted using beams made of three asphalt layers with grids between them, below and above the neutral axis. Even fewer studies investigated specimens made up of a single layer with a grid adhered to the specimens' bottom [15]. Most test specimens typically consisted of two asphalt layers with a grid between them [3, 6, 13, 14, 37, 38], usually in the tension zone, below the neutral axis, as suggested by Zofka et al. [3]. A more sophisticated approach has been used in other studies [8, 9, 16, 23], where notches of various dimensions were made at the middle of the bottom specimen's side to simulate the existence of cracks in the field. In one study [10] the grid was placed in the middle of the specimen, i.e. in the neutral zone. Kumar and Saride [7] went further



in simulating field conditions and produced test specimens in the laboratory conditions, where a lower layer of old asphalt was excavated from the field on the top of which was placed geogrid and a thicker layer of new asphalt.

The method by which the effectiveness of the grid will be assessed should be chosen after the test method and the type of test specimen have been chosen, even though the officially accepted term for that lacks current usage. Several terms serve the similar purpose: traffic benefit ratio—TBR [39], effectiveness benefit ratio—EBR [31], grid efficiency factor—GEF [10], improvement ratio—IR [38], improvement factor—IF [6], interlayer crack performance factor—ICPF [23] and performance coefficient— $k$  [19]. Each of them is based on the same principle, comparing the various properties of grid-reinforced asphalt specimens to those of unreinforced specimens (such as rutting, cracking, or fatigue resistance).

If fatigue resistance is selected as the performance based on which the effectiveness of the network is assessed, the methodology and established criteria used to analyze the test results can have a significant impact on the outcomes. There are several criteria used to accomplish that: stiffness reduction criterion (50% [40] or even 90% reduction [41]), phase angle criterion [42] and dissipated energy criteria [43–45]. Similarly to the case of single-layered specimens [46], the application of different criteria on the same dataset can result in even more varied fatigue laws when the asphalt specimens contain a grid reinforcement [47]. In one study, it was even suggested that when grid reinforcement is utilized, a new analysis criterion of failure should be developed and used instead of the traditional approach (50% stiffness reduction) [36]. To overcome the shortcomings due to the unreliable selection of the number of cycles to failure, Virgili et al. [38] used the permanent deformation evolution model—PDEM to define the permanent deformation evolution of a specimen during a repeated load test, from which the number of loading cycles corresponding to the flex point of the curve was selected as the failure criterion. This approach is very reasonable because it has been proven that the reduction of pavement deflections due to the geogrid application might lead to a significant extension of pavement fatigue life [3]. However, when geogrids are used as reinforcement, none of these criteria has yet been broadly adopted and standardized.

Consequently, the paper presents a newly developed approach for estimating the fatigue life utilizing the 4PBB fatigue test results. The developed methodology was applied to the test results of four different double-layered sets prepared for the purposes of this study. In addition to one unreinforced, laboratory tests were carried out on three sets reinforced with various geogrids. Fatigue lives of all sets were determined using the newly-developed approach and then compared to the results obtained by using the traditional and the energy ratio (ER) approach (considering reduced energy ratio, i.e. normalized stiffness modulus  $\times$  number of repetitions).

## 2 Materials and method

The experimental program included four double-layered sets: a set of specimens without reinforcement and three sets with different geogrids applied between layers. The first research stage consisted of sampling the asphalt mixture directly from an asphalt plant's hot storage bin, compacting the slabs, and then cutting the slabs to produce test specimens (beams). Volumetric properties and fatigue resistance of all specimens were determined in the second stage, whereas data analysis was performed in the third stage utilizing three alternative approaches. The remainder of this chapter provides information related to materials' properties and applied methodologies, while Fig. 1 summarizes the experimental plan of the study.

### 2.1 Materials

#### 2.1.1 Asphalt mixture

A typical asphalt mixture for surface layers (AC 11 surf) prepared with plain 50/70 penetration grade bitumen and the gradation curve displayed in Fig. 2 was selected for the experimental program. To minimize potential variability, the entire amount of material needed for the study was sampled on the same day from a single hot storage bin of an asphalt plant. Table 1 shows the components of asphalt mixtures along with their proportions, whereas Table 2 shows the physical–mechanical properties of the asphalt mixture.

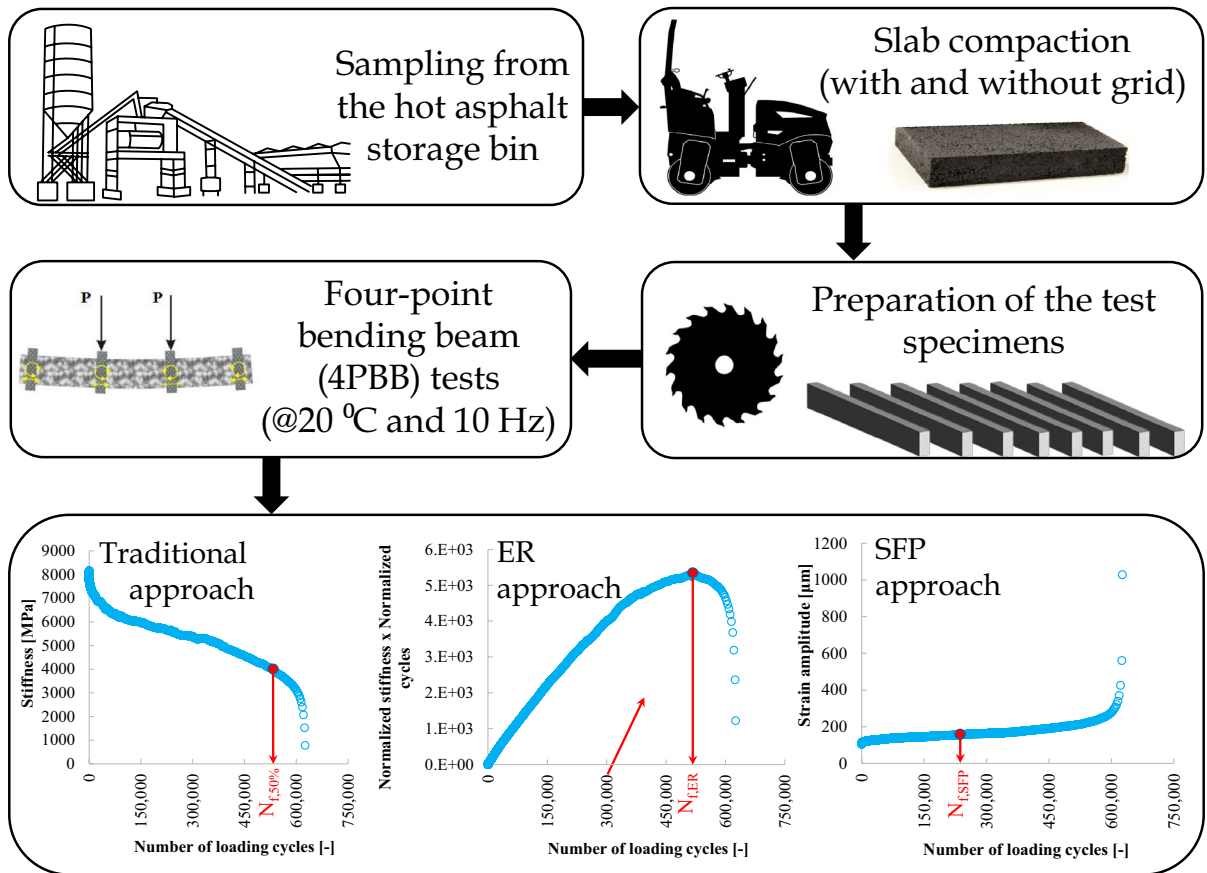


**Fig. 1** Experimental plan of the study

**Table 1** Proportions of the component materials in the mixture

Material type	Amount [%]
Limestone filler	5.5
Limestone aggregate fraction 0/2 mm	27.6
Igneous aggregate fraction 2/4 mm	15.7
Igneous aggregate fraction 4/8 mm	25.6
Igneous aggregate fraction 8/11 mm	20.6
Bitumen BIT 50/70	5.0

### 2.1.2 Reinforcement

Three polymer-coated fiberglass geogrids (Fig. 3) with different longitudinal and transversal strengths (50×50, 100×100, and 100×200 kN/m coded as G1, G2 and G3, respectively), were used in this study. The mesh size opening of the first two geogrids was

25×25 mm, whereas the third one was 25×19 mm. Each grid had an adhesive layer on the bottom side, which secured the adhesion of the grid to the surface during installation and paving.

Bitumen emulsion KN-60 (cationic bitumen emulsion with 60% residual binder) was used as a tack coat in this study, even though the manufacturer recommends the use of emulsion with a minimum 65% residual binder. Regardless of whether the grid was used or not, 300 g/m<sup>2</sup> of the bitumen emulsion was applied between the upper and the lower AC layer.

## 2.2 Methods

### 2.2.1 Specimens' preparation

All test specimens were carefully prepared following the same procedure because their quality can have a major impact on the test results. After sampling the



**Table 2** Physical–mechanical properties of the asphalt mixture

Properties	Unit	Standard	Results	Criterion <sup>a</sup>
Stability–S	kN	EN 12697–34	10.4	min 8
Flow–F	mm		3.5	–
Marshall quotient–S/F	kN/mm		3.0	min 2
Bulk density	Mg/m <sup>3</sup>	EN 12697–6	2.428	–
Maximum density	Mg/m <sup>3</sup>	EN 12697–5	2.558	–
Air void content	% [v/v]	EN 12697–8	5.1	4.5–5.5
Voids in mineral aggregated filled with binder	% [v/v]	EN 12697–8	69.9	66–78
Voids in mineral aggregate	% [v/v]	EN 12697–8	16.9	–

<sup>a</sup>SRPS U.E4.014: Technical specifications for asphalt concrete pavements

**Fig. 2** The gradation curve of the asphalt mixture

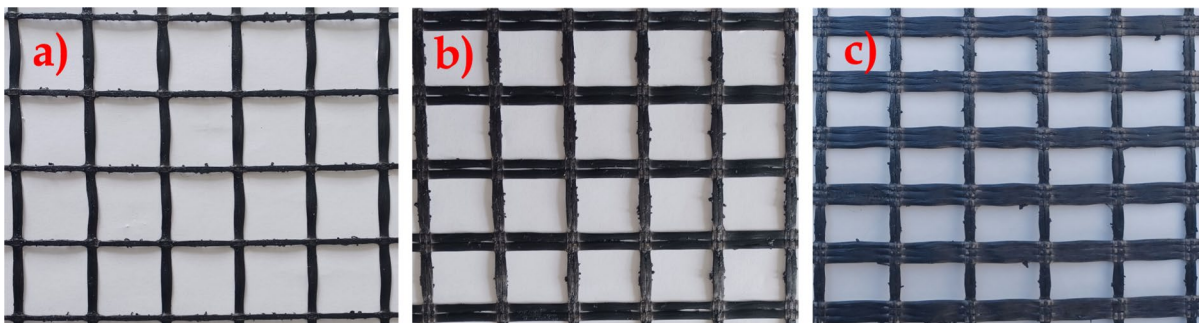
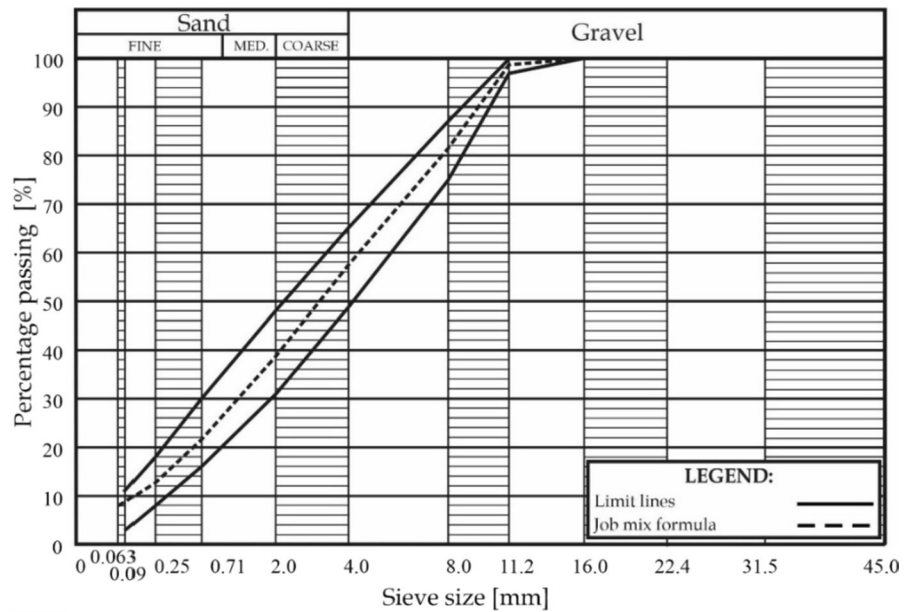


**Fig. 3** The fiberglass geogrids used in the study: (a) G1, (b) G2 and (c) G3

asphalt mixture from the asphalt plant, a 1-ton roller was used to compact twelve slabs (three per each set),

with dimensions of 50×50×7 cm, in metal molds. Slab compaction was performed in two stages. In

the first stage, the 3-cm thick bottom layer was initially compacted and after the asphalt mixture had been cooled down, the bitumen emulsion was applied and let to break. When geogrids were used, they were placed on and pressed by several roller passes to ensure adhesion between the grid and the asphalt surface. In the second stage, the 4 cm thick upper layer was paved. The day after the compaction of the second layer, slabs were removed from molds and sawed to obtain six beams from each slab (in total 18 beams). The beams were 6 cm wide and 40 cm long. The total height of each beam was 5 cm, including 2 cm of the bottom layer and 3 cm of the upper layer. This means that the interfaces (containing tack coat only or tack coat and geogrid) were below the neutral zone - in the tension zone. The whole procedure of specimens' preparation is shown in Fig. 4.

### 2.2.2 Performance evaluation

Before the start of the fatigue tests, the bulk density of each saturated surface dry specimen was determined (EN 12697-6/B:2020), and consequently, air void content was calculated following EN 12697-8:2019.

The initial stiffness modulus and phase angle of each beam were measured in accordance with EN 12697-26/B:2018, using a 4PBB device. The tests were performed at a temperature of 20 °C and frequencies of 0.1, 1, 5, 8 and 10 Hz. Specimens were

subjected to 100 sinusoidal load cycles with a constant strain amplitude of  $(50 \pm 3) \mu\epsilon$ .

Fatigue resistance of all specimens was determined using the 4PBB test, at a single temperature of 20 °C and a frequency of 10 Hz, according to EN 12697-24/D:2018. Before being loaded, the specimens were conditioned for at least 2 h at a testing temperature. Tests were performed in the stress-controlled mode because of the rapid strain increase during the test that causes faster crack propagation, consequently allowing easier determination of the failure occurrence [6]. Tests were carried out at three stress levels, where six beams of each set were tested per each level so that all fatigue failures occur in the range from  $10^4$  to  $10^6$  loading cycles.

### 2.2.3 Data analysis

The results of each specimen from a certain set (number of loading cycles and initial strain value) were fitted together and presented in the form of a power (fatigue) function:

$$\log(N_{i,j,k}) = A_0 + A_1 \cdot \log(\epsilon_i) \quad (1)$$

where  $i$  is the specimen number,  $j$  is the chosen failure criteria,  $k$  is the set of test conditions (20 °C and 10 Hz),  $\epsilon_i$  is the initial strain amplitude measured at the 50th or 100th load cycle ( $\mu\text{m/m}$ ), depending

**Fig. 4** Preparation of the test specimens



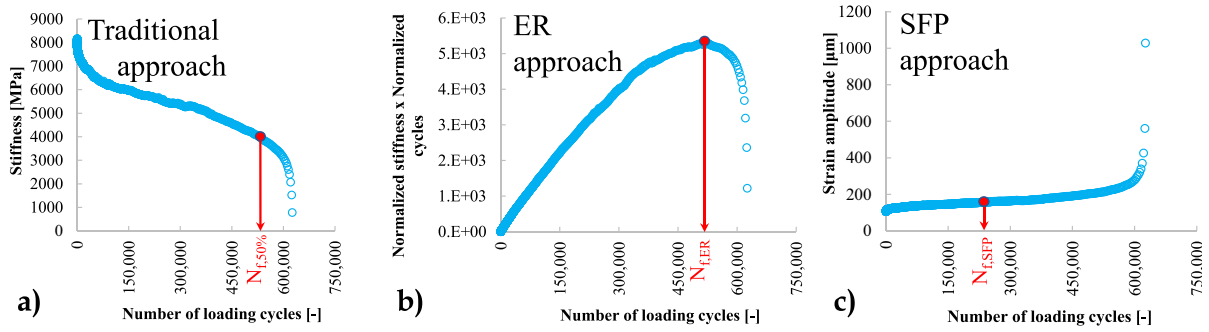


**Fig. 5** Failure criteria used for fatigue analysis: (a) the traditional approach, (b) the ER approach and (c) the SFP approach

on the failure criteria,  $A_1$  is the slope of the fatigue function in the log–log plot, and  $A_0$  is the fitting parameter.

In this study, three different failure criteria (approaches) were used to determine fatigue lives: the traditional, the ER and the newly developed SFP approach. Fatigue laws were obtained using Eq. 1, from which critical strain  $\epsilon_6$ , that leads to fatigue failure after  $10^6$  cycles, was calculated and then used for comparison of the fatigue lives among different sets and approaches applied.

**2.2.3.1 The traditional approach** Van Dijk and Visser [48] defined the failure under cyclic loading as the point at which the stiffness drops to 50% of its initial value, which is typically regarded as the stiffness at the 100th cycle ( $N_{f,50\%}$ , Fig. 5a). Although this method is straightforward, it has some limitations. The estimation of the initial value based on the number of cycles may be affected by nonlinearity [49], irreversible damage and thixotropy [50]. Furthermore, true failure of a test specimen often occurs between 35 and 65% stiffness decrease, although it can occur as low as 20% of initial stiffness for heavily modified materials [51]. Despite its limitations, this approach has often been used in previous studies [52, 53], and it is a part of the European standard for fatigue resistance EN 12697–24:2018, therefore it was selected as one of the approaches in this study.

**2.2.3.2 energy ratio approach** Hopman et al. [54] proposed the failure in a strain-controlled testing mode as the number of cycles ( $N_1$ ) up to the point at which cracks are considered to initiate and defined the energy ratio (ER) as:

$$R_E = \frac{nW_0}{W_n} = \frac{n[\pi\sigma_0\epsilon_0\sin\varphi_0]}{\pi\sigma_n\epsilon_n\sin\varphi_n} \quad (2)$$

where  $n$  is the number of cycles,  $W_0$  and  $W_n$  are the dissipated energy in the first and  $n$ -th cycle, respectively,  $\sigma_0$  and  $\sigma_n$  are stress levels in the first and  $n$ -th cycle,  $\epsilon_0$  and  $\epsilon_n$  are strain levels in the first and  $n$ -th cycle, respectively, and  $\varphi_0$  and  $\varphi_n$  are phase angles in the first and  $n$ -th cycle, respectively.

Rowe [41] stated that the change in  $\sin\varphi$  is small compared to the change in the complex modulus ( $E_i^*$ ) and therefore simplified equation for calculating the ER ( $R_\sigma$ ) in a stress-controlled mode:

$$R_\sigma \cong nE_i^* \quad (3)$$

where  $n$  is the number of load cycles and  $E_i^*$  is the complex modulus in the  $n$ -th cycle [MPa].

A slightly modified approach is adopted in the standard ASTM D8237-21, where the failure ( $N_{f,ER}$ ) is defined as the maximum value of normalized stiffness x normalized cycles versus a number of cycles plot (Fig. 5b), which is calculated according to the following equation:

$$\hat{S} \times \hat{N} = \frac{S_i \times N_i}{S_0 \times N_0} \quad (4)$$

where  $\hat{S} \times \hat{N}$  is normalized beam stiffness x normalized cycles,  $S_i$  is flexural beam stiffness at cycle  $i$  (MPa),  $N_i$  is cycle  $i$ ,  $S_0$  is initial flexural beam stiffness (MPa), estimated at approximately 50th cycle, and  $N_0$  is actual cycle number where initial flexural beam stiffness is estimated.

The calculated normalized stiffness data can be fit to a six-order polynomial curve or Logit model,



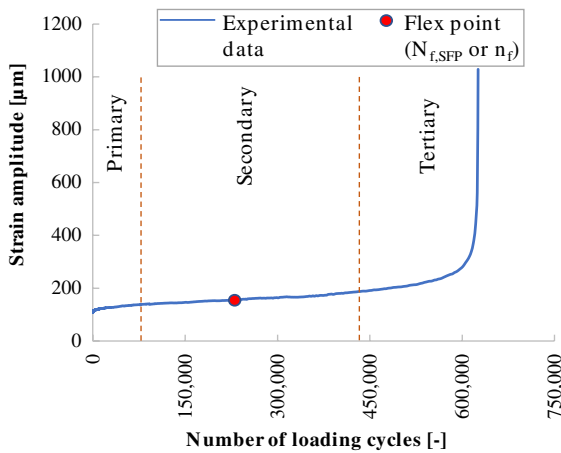


**Fig. 6** Three-stages experimental curve of the strain amplitude evolution

ensuring easy determination of the failure. Therefore, it was decided to employ this method as it is frequently used to evaluate the fatigue failure of specimens in the 4PBB setup and also being a part of ASTM D8237-21 standard.

**2.2.3.3 The simplified flex point approach** The curve  $\varepsilon(n)$  representing the strain amplitude evolution in control load conditions consists of a succession of experimental data in terms of a number of loading cycles and corresponding deformation level (Fig. 5c). The acquired loading cycles are numerically very close at the beginning of the test and then become progressively more distant, even irregularly, during the test, mostly because of the machine's limitations. This condition is detrimental to the application of a finite difference method (both linear and non-linear).

The experimental curve of strain amplitude evolution under repeated loading cycles (Fig. 6) has three typical stages (primary, secondary and tertiary stage) with completely different experimental trends. In these stages, the strain amplitude rate (slope of the curve) is always positive and in the primary stage, it decreases rapidly. In the secondary stage, the strain amplitude evolution curve has an inflexion, namely flex point ( $N_{f,SFP}$ ), which is assumed as a reference for identifying the fatigue resistance of the material tested. In the tertiary stage of the curve, the deformation rate increases rapidly till the physical failure of the specimen is reached.

From these considerations, it can be concluded how difficult is to find a robust and simple interpolation method to identify the flex point of the strain amplitude curve, which is the main outcome of so-called SFP approach. An interpolation method using a non-linear polynomial of suitable order (single or segmented) is not helpful in this case, given the fact that the curve in the secondary stage theoretically could have a waving trend with a certain number of flex points instead of the single flex point suggested by the experimental data (except for their small intrinsic scattering). Furthermore, a high-order polynomial (up to 7th order) would be required to adequately model the primary and tertiary stages. To solve the above computational issues, a dedicated non-linear interpolation method was developed, considering the main characteristics of the experimental strain amplitude evolution curve.

This curve always has the following characteristics:

- the curve is strictly increasing, therefore the slope is always positive;
- the second derivative (related to the curvature) is always negative for the points preceding the flex point and positive for the subsequent ones;
- the third derivative is positive along the whole curve (i.e. the curvature is increasing).

Based on these features, a high-order nonlinear polynomial can be used to set up an interpolation method that complies with the characteristics of the experimental curve by imposing some unilateral and bilateral constraints on its constant parameters.

The theoretical model of the strain amplitude  $\varepsilon(n)$  can be described by the following polynomial of  $N$ -order, where  $n$  indicates the generic position along the curve and  $n_f$  denotes the location of the flex point:

$$\varepsilon(n) = \sum_{i=0}^N K_i (n - n_f)^i \quad (5)$$

where  $K_i$  indicates the constants of the model of  $N$ -order, which are equal to  $N + 1$ .

The model is completed by adding to Eq. 5 the following conditions:

- I. The slope is non-negative for any value of  $n$ ;





$$\frac{d\varepsilon(n)}{dn} = \sum_{i=1}^N iK_i(n - n_f)^{i-1} \geq 0 \tag{6}$$

II. The curvature is non-negative for values of  $n$  greater than  $n_f$  and negative for the  $n$  values lower than  $n_f$ ;

$$\frac{d^2\varepsilon(n)}{dn^2} = \sum_{i=2}^N i(i-1)K_i(n - n_f)^{i-2} \leq 0 : n \geq n_f \tag{7}$$

III. The third derivative is non-negative for any value of  $n$ .

$$\frac{d^3\varepsilon(n)}{dn^3} = \sum_{i=3}^N i(i-1)(i-2)K_i(n - n_f)^{i-3} \geq 0 \tag{8}$$

From a theoretical point of view, the problem is solved by determining the constants  $K_i$  in Eq. 5 by using the least squares method and satisfying the unilateral constraints (Eqs. 6–8). For this purpose, a constrained least squares method is used, so these constraints are polynomial inequalities of  $N - 1$ ,  $N - 2$  and  $N - 3$  order, respectively. By calculating them in the flex point  $n_f$  it is obtained:

$$\frac{d\varepsilon(n_f)}{dn} = K_1 \geq 0 \tag{9}$$

$$\frac{d^2\varepsilon(n_f)}{dn^2} = 2K_2 \leq 0 : n \geq n_f \rightarrow K_2 = 0 \tag{10}$$

$$\frac{d^3\varepsilon(n_f)}{dn^3} = 6K_3 \geq 0 \tag{11}$$

Therefore, both  $K_1$  and  $K_3$  must be non-negative, whereas  $K_2$  must be equal to zero.

By replacing Eq. 10 in Eq. 7 and taking the term  $(n - n_f)$  out of the summation, the constraint from Eq. 7 can be written as:

$$\frac{d^2\varepsilon(n)}{dn^2} = (n - n_f) \sum_{i=3}^N i(i-1)K_i(n - n_f)^{i-3} \leq 0 : n \geq n_f \tag{12}$$

which can be simplified by dividing by  $(n - n_f)$ , thus obtaining:

$$\sum_{i=3}^N i(i-1)K_i(n - n_f)^{i-3} \geq 0 \tag{13}$$

In summary, the algorithm that solves the problem consists of the search for a constrained minimum. The minimum of the sum of the squared deviations between the values  $\varepsilon(n)$  provided by the model given in Eq. 5 and the corresponding experimental values,  $\varepsilon$  will be sought, in compliance with Eq. 10 and inequalities provided in Eqs. 6, 8, 9, 11 and 13.

### 2.2.4 Fatigue resistance improvement factor

The impact of grid reinforcement on the fatigue evaluation was assessed using the newly introduced fatigue resistance improvement factor (FRIF), given that critical strain was employed as an indicator of the fatigue resistance of the asphalt mixtures. Positive FRIF values, calculated according to Eq. 14, mean that reinforced set have improved fatigue resistance when compared to the unreinforced, and opposite.

$$FRIF = \frac{\varepsilon_6^R - \varepsilon_6^{UR}}{\varepsilon_6^{UR}} \times 100 \tag{14}$$

where  $\varepsilon_6^R$  is the critical strain value of a reinforced set and  $\varepsilon_6^{UR}$  is the corresponding critical strain value of an unreinforced set.

## 3 Results and discussion

### 3.1 Basic properties of the test specimens

The average air void content of eighteen test specimens of each set, as well as the minimum and maximum values measured, are given in Fig. 7. Although the unreinforced set (UR) had the biggest variation in measured values, average values of all sets were within the range of  $7 \pm 1\%$ , ensuring a trustworthy comparison of the test results. It can also be observed that sets reinforced with the geogrids (noted as G1, G2 and G3, depending on the grid applied) have a slightly increased air void content, confirming the results from the previous study [36].

When stiffness values are considered (Fig. 8), it is evident that the higher air void content resulting from the usage of geogrids caused a stiffness reduction. These results are in agreement with recent



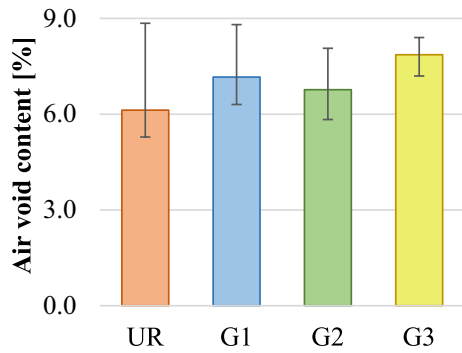


**Fig. 7** Air void content of the test specimens

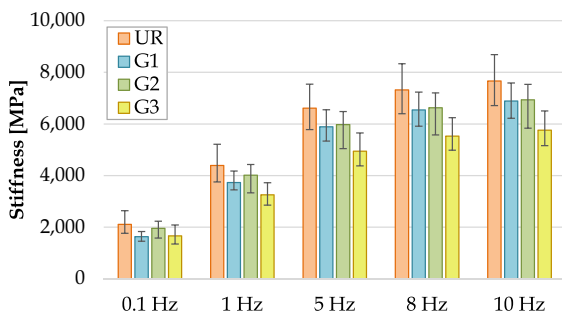


**Fig. 8** Stiffness of the testing sets at different frequencies

findings [36, 55] that the stiffness increases with a decrease in air void content and vice versa, regardless of the testing frequency. Moreover, it should be taken into account that in the case of double-layered specimens air void distribution is not uniform, having a larger content at the interface [56]. This effect is even more amplified in the presence of geogrids that may cause the debonding effect with direct influence on the overall specimen stiffness. The test results further demonstrate that the stiffness and the variation in measured values were unaffected by the strength of the geogrid.

### 3.2 Fatigue laws of the investigated sets

The number of cycles to failure calculated using the different approaches at the selected stress levels was fitted with the power function (Eq. 1). Regression coefficients  $A_0$  and  $A_1$ , as well as the coefficient of correlation  $R^2$  were also calculated for each approach (Table 3). Finally, critical strain values  $\epsilon_6$  were calculated for comparison purposes among different approaches and geogrid types (Fig. 9).

The critical strain value calculated using the SFP approach is always the smallest, whereas the values obtained using the traditional and ER approaches are comparable, apart from specimens reinforced with the G2 grid. The correlation coefficient estimated using the traditional approach was reasonably high (above 0.8) but not comparable to those obtained using the other two approaches, providing a substantially lower  $\epsilon_6$  value. Nevertheless, it is well known that laboratory conditions are never equal to a real-scale pavement performance. Therefore, the use of fatigue cracking transfer functions [57] is always necessary to adjust laboratory-determined  $\epsilon_6$  values of reinforced asphalt systems for pavement design purposes, regardless of the approach applied.

The test results, except those of the set reinforced with the G2 grid obtained using the traditional approach, show that reinforcement improves fatigue resistance. When considering the traditional approach, critical strain  $\epsilon_6$  value of the set reinforced with the G3 grid was higher by roughly 9% compared to that of the G1 set. According to the results of the ER analysis, the critical strain value rises as grid strength increases, whereas in the case of the SFP approach, the highest critical strain value was found in the G2 set, being just slightly higher than that of the G3 set.

When looking at the results of G2 and G3 sets shown in Fig. 9, it can be seen that the differences between  $\epsilon_6$  values for both ER and SFP approaches

**Table 3** Regression coefficients of fatigue laws and coefficients of correlation

	UR			G1			G2			G3		
	50%	ER	SFP	50%	ER	SFP	50%	ER	SFP	50%	ER	SFP
$A_0$	16.48	16.72	16.33	16.38	16.38	15.94	16.21	18.68	18.67	16.72	16.30	15.77
$A_1$	-5.26	-5.38	-5.34	-5.14	-5.15	-5.08	-5.15	-6.16	-6.26	-5.21	-4.98	-4.85
$R^2$	0.98	0.98	0.98	0.98	0.98	0.98	0.82	0.91	0.91	0.94	0.97	0.97



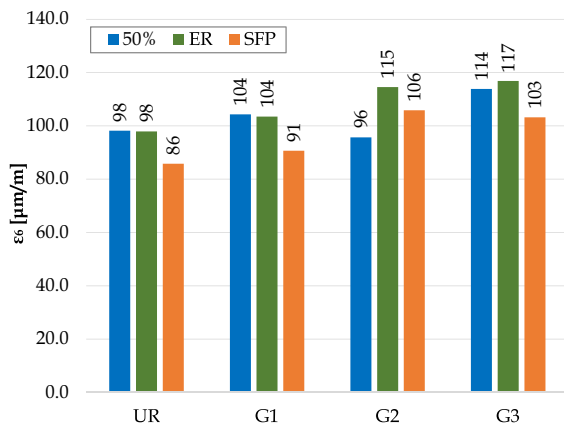


**Fig. 9** Critical strain values obtained using different approaches

are quite low (ER: 115 vs. 117  $\mu\text{m/m}$ ; SFP: 106 vs. 103  $\mu\text{m/m}$ ) and could be within the experimental uncertainty range. In general, based on the research outcomes, the maximum strength of the geogrid able to increase the fatigue performance seems to be 100 kN (i.e. G2). The higher benefit of using the strongest grid (i.e., G3) is most likely limited due to the shear bond. As this grid is the stiffest of all the grids used in this study, it would be more advantageous to apply a higher amount of the same tack coat or a tack coat with polymer-modified bitumen and a higher residual bitumen percentage than the one used in this study to completely utilize its efficacy [58]. Moreover, the cross-dimensional area of 200 kN geogrids could also be detrimental to the interlayer bonding between asphalt layers with a negative impact on the overall fatigue performance of a layered pavement, highlighting the importance of using an appropriate tack coat type and amount. These conclusions could explain the decrease of the critical strain  $\epsilon_6$  values that emerged with the SFP approach when comparing the results of G2 and G3 sets.

### 3.3 Fatigue resistance improvement factor

The FRIF values are displayed in Fig. 10. In general, almost all sets, except G2, have positive values, meaning that reinforcement improves fatigue resistance, as it was proven in previous studies [3, 10].

The average improvement in fatigue resistance of the G1 set was around 5.8%, regardless of the approach applied. The use of the G3 geogrid

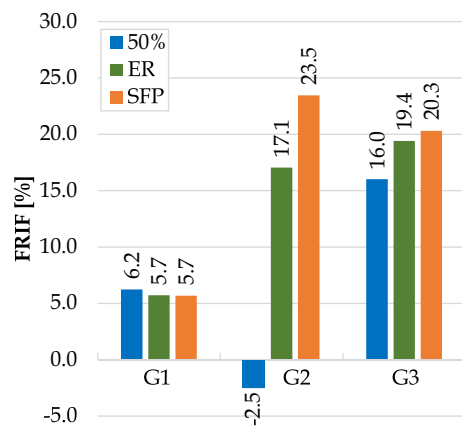


**Fig. 10** Fatigue resistance improvement factors of testing sets

caused an improvement of 16% when the traditional approach was used, followed by 19.4% and 20.3% when the ER and SFP approaches were used. The highest discrepancy between the FRIF values was found in the case of the G2 set, where was a clear improvement in fatigue life from 17.1% (ER approach) to 23.5% (SFP approach), whereas the traditional approach showed no improvement but rather a worsening of fatigue resistance.

One possible reason for the unreliability of the traditional approach can be related to the damage condition associated with this method which is stress-sensitive as opposed to the other two approaches. For example, when looking at Fig. 11, it is clear that the number of cycles to failure related to the SFP approach is always close to the midrange of the secondary phase, regardless of the stress level, whereas in the case of the traditional approach, the damage associated to the number of cycles to failure is stress sensitive. Specifically, for the traditional approach the output of the fatigue failure becomes closer to the tertiary phase for lower stress level (Fig. 11b), when compared to the higher stress level (Fig. 11a). This has already been identified as a potential problem with this method [41], especially when highly modified bitumen is used [51].

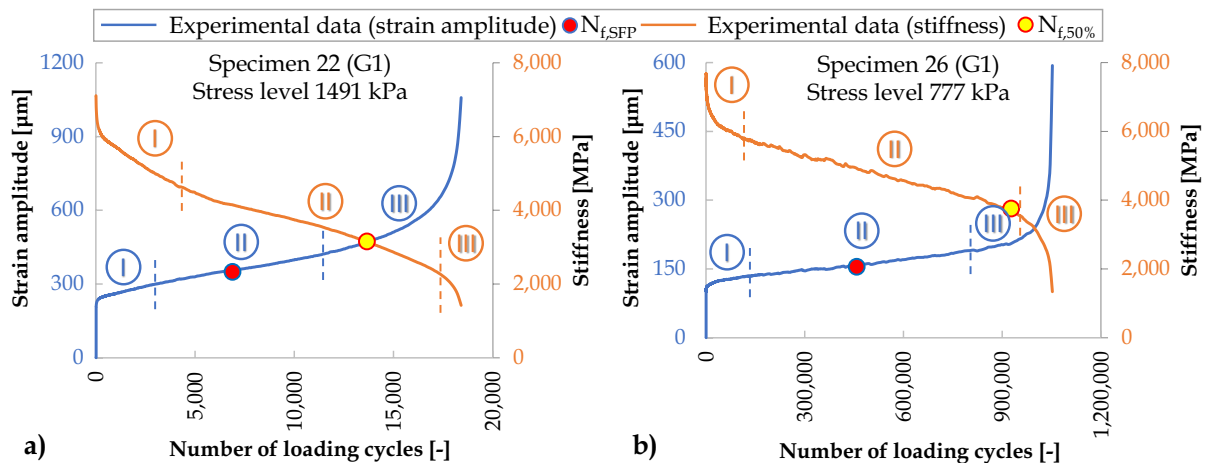


**Fig. 11** Stress sensitivity of the traditional approach compared to the SFP approach

#### 4 Conclusions

The behaviour of reinforced double-layered asphalt specimens has been a topic of numerous research studies because of their complexity and various grid types used. The approach that should be utilized for their fatigue analysis is not yet established, in contrast to single-layer specimens, where the traditional (50% reduction in initial stiffness) and the energy ratio (ER) approaches are already implemented in suitable standards (EN 12697-24:2018 and ASTM 8237-21). Therefore, the simplified flex point (SFP) approach, that analyses the strain amplitude curve obtained during the fatigue test, is developed in this study. After applying these three approaches to the 4PBB fatigue test results of one unreinforced set and three sets reinforced with various geogrids, the results were further compared to each other, leading to the subsequent conclusions:

- The grid reinforcement improves the fatigue resistance in terms of critical strain in the range of 5.7–22.3%, depending on the grid type and the approach used in the study. The only exception appeared in the case of the traditional approach, which indicated that the G2 geogrid allegedly decreases fatigue resistance.
- Critical strain values obtained using the SFP approach are always lower than those obtained using the traditional and ER approaches.

- The FRIF values showed that the newly developed SFP approach has quite comparable results with those from the ER approach.
- When testing reinforced specimens, the application of traditional approach should be avoided because it may underestimate a grid efficiency.

The newly developed approach could be utilized to examine the effectiveness of the various geogrids (for example, geocomposite), test temperature and tack coat type and content on the fatigue resistance. Additionally, the behaviour of asphalt mixtures comprising grid reinforcement, polymer-modified bitumen and tack coat may be much more complex, thus the applicability of this approach should also be investigated.

**Funding** Open access funding provided by Università Politecnica delle Marche within the CRUI-CARE Agreement.

**Open Access** This article is licensed under a Creative Commons Attribution 4.0 International License, which permits use, sharing, adaptation, distribution and reproduction in any medium or format, as long as you give appropriate credit to the original author(s) and the source, provide a link to the Creative Commons licence, and indicate if changes were made. The images or other third party material in this article are included in the article's Creative Commons licence, unless indicated otherwise in a credit line to the material. If material is not included in the article's Creative Commons licence and your intended use is not permitted by statutory regulation or exceeds the permitted use, you will need to obtain permission directly from the copyright holder. To view a copy of this licence, visit <http://creativecommons.org/licenses/by/4.0/>.



## References

- Koerner RM (2005) Designing with geosynthetics. pearson prentice hall upper saddle river, NJ, USA
- Zornberg JG (2017) Functions and applications of geosynthetics in roadways. *Procedia Eng* 189:298–306. <https://doi.org/10.1016/j.proeng.2017.05.048>
- Zofka A, Maliszewski M, Maliszewska D (2017) Glass and carbon geogrid reinforcement of asphalt mixtures. *Road Mater Pavement Des* 18:471–490. <https://doi.org/10.1080/14680629.2016.1266775>
- Zamora-Barraza D, Calzada-Pérez MA, Castro-Fresno D, Vega-Zamanillo A (2011) Evaluation of anti-reflective cracking systems using geosynthetics in the interlayer zone. *Geotext Geomembranes* 29:130–136. <https://doi.org/10.1016/j.geotexmem.2010.10.005>
- Walubita LF, Faruk ANM, Zhang J, Hu X (2015) Characterizing the cracking and fracture properties of geosynthetic interlayer reinforced HMA samples using the overlay tester (OT). *Constr Build Mater* 93:695–702. <https://doi.org/10.1016/j.conbuildmat.2015.06.028>
- Sudarsanan N, Arulrajah A, Karpurapu R, Amrithalingam V (2020) Fatigue performance of geosynthetic-reinforced asphalt concrete beams. *J Mater Civ Eng* 32:1–13. [https://doi.org/10.1061/\(asce\)mt.1943-5533.0003267](https://doi.org/10.1061/(asce)mt.1943-5533.0003267)
- Kumar V, Saride S (2017) Use of digital image correlation for the evaluation of flexural fatigue behavior of asphalt beams with geosynthetic interlayers. *Transp Res Rec* 2631:55–64. <https://doi.org/10.3141/2631-06>
- Wargo A, Safavizadeh SA, Richard Kim Y (2017) Comparing the performance of fiberglass grid with composite interlayer systems in asphalt concrete. *Transp Res Rec* 2631:123–132. <https://doi.org/10.3141/2631-14>
- Jaskula P, Rys D, Stienss M et al (2021) Fatigue performance of double-layered asphalt concrete beams reinforced with new type of geocomposites. *Materials (Basel)* 14:1409. <https://doi.org/10.3390/ma14092190>
- Lee SY, Phan TM, Park DW (2022) Evaluation of carbon grid reinforcement in asphalt pavement. *Constr Build Mater* 351:128954. <https://doi.org/10.1016/j.conbuildmat.2022.128954>
- Mirzapour Mounes S, Karim MR, Khodaii A, Almasi MH (2014) Improving rutting resistance of pavement structures using geosynthetics: an overview. *Sci World J*. <https://doi.org/10.1155/2014/764218>
- Pasquini E, Bocci M, Ferrotti G, Canestrari F (2013) Laboratory characterisation and field validation of geogrid-reinforced asphalt pavements. *Road Mater Pavement Des* 14:17–35. <https://doi.org/10.1080/14680629.2012.735797>
- Shafabakhsh G, Akbari M, Bahrami H (2020) Evaluating the fatigue resistance of the innovative modified-reinforced composite asphalt mixture. *Adv Civ Eng*. <https://doi.org/10.1155/2020/8845647>
- Ferrotti G, Canestrari F, Virgili A, Grilli A (2011) A strategic laboratory approach for the performance investigation of geogrids in flexible pavements. *Constr Build Mater* 25:2343–2348. <https://doi.org/10.1016/j.conbuildmat.2010.11.032>
- Darzins T, Qiu H, Xue J (2021) A preliminary laboratory study of fatigue performance of geogrid-reinforced asphalt beam. In: Steyn W, Wang Z, Holleran G (eds) civil infrastructures confronting severe weathers and climate changes conference. Springer International Publishing, pp 67–77
- Safavizadeh SA, Wargo A, Guddati M, Kim YR (2015) Investigating reflective cracking mechanisms in grid-reinforced asphalt specimens: Use of four-point bending notched beam fatigue tests and digital image correlation. *Transp Res Rec* 2507:29–38. <https://doi.org/10.3141/2507-04>
- Raab C, Arraigada M, Partl MN, Schiffmann F (2017) Cracking and interlayer bonding performance of reinforced asphalt pavements. *Eur J Environ Civ Eng* 21:14–26. <https://doi.org/10.1080/19648189.2017.1306462>
- Ragni D, Canestrari F, Allou F et al (2020) Shear-torque fatigue performance of geogrid-reinforced asphalt interlayers. *Sustain* 12:143. <https://doi.org/10.3390/su1214381>
- Ingrassia LP, Virgili A, Canestrari F (2020) Effect of geocomposite reinforcement on the performance of thin asphalt pavements: Accelerated pavement testing and laboratory analysis. *Case Stud Constr Mater* 12:e00342. <https://doi.org/10.1016/j.cscm.2020.e00342>
- Nguyen ML, Blanc J, Kerzrého JP, Hornych P (2013) Review of glass fibre grid use for pavement reinforcement and APT experiments at IFSTTAR. *Road Mater Pavement Des* 14:287–308. <https://doi.org/10.1080/14680629.2013.774763>
- Nguyen ML, Hornych P, Le XQ et al (2021) Development of a rational design procedure based on fatigue characterisation and environmental evaluations of asphalt pavement reinforced with glass fibre grid. *Road Mater Pavement Des* 22:S672–S689. <https://doi.org/10.1080/14680629.2021.1906304>
- Nielsen J, Levenberg E (2022) Full-scale validation of a mechanistic model for asphalt grid reinforcement. *Int J Pavement Eng* 80:1–19. <https://doi.org/10.1080/10298436.2023.2220064>
- Walubita LF, Nyamuhokya TP, Torres POL et al (2020) Laboratory evaluation of grid-reinforced HMA beams using the flexural bending-beam fatigue (FBBF) test in load-controlled mode. *Int J Pavement Eng* 20:1–15. <https://doi.org/10.1080/10298436.2020.1795659>
- Freire R, Di Benedetto H, Sauzéat C et al (2023) Rational design method for bituminous pavements reinforced by geogrid. *Geotext Geomembranes* 51:39–52. <https://doi.org/10.1016/j.geotexmem.2023.04.008>
- Cleveland GS, Button JW, Lytton RL (2002) Geosynthetics in flexible and rigid pavements overlay systems to reduce reflection cracking. College Station, Texas
- Kumar VV, Roodi GH, Subramanian S, Zornberg JG (2023) Installation of geosynthetic interlayers during overlay construction: case study of texas state highway 21. *Transp Geotech* 43:101127. <https://doi.org/10.1016/j.trgeo.2023.101127>
- Yang K, Li R (2021) Characterization of bonding property in asphalt pavement interlayer: a review. *J Traffic Transp Eng (English Ed)* 8:374–387. <https://doi.org/10.1016/j.jtte.2020.10.005>
- Romeo E, Montepara A (2012) Characterization of reinforced asphalt pavement cracking behavior using flexural



- analysis. *Procedia - Soc Behav Sci* 53:356–365. <https://doi.org/10.1016/j.sbspro.2012.09.887>
29. Sudarsanan N, Karpurapu R, Amirthalingam V (2019) Investigations on fracture characteristics of geosynthetic reinforced asphalt concrete beams using single edge notch beam tests. *Geotext Geomembranes* 47:642–652. <https://doi.org/10.1016/j.geotextmem.2019.103461>
  30. Arsenie IM, Chazallon C, Duchez JL, Hornych P (2016) Laboratory characterisation of the fatigue behaviour of a glass fibre grid-reinforced asphalt concrete using 4PB tests. *Road Mater Pavement Des* 18:168–180. <https://doi.org/10.1080/14680629.2016.1163280>
  31. Tam AB, Park DW, Le THM, Kim JS (2020) Evaluation on fatigue cracking resistance of fiber grid reinforced asphalt concrete with reflection cracking rate computation. *Constr Build Mater* 239:117873. <https://doi.org/10.1016/j.conbuildmat.2019.117873>
  32. Gonzalez-Torre I, Calzada-Perez MA, Vega-Zamánillo A, Castro-Fresno D (2015) Evaluation of reflective cracking in pavements using a new procedure that combine loads with different frequencies. *Constr Build Mater* 75:368–374. <https://doi.org/10.1016/j.conbuildmat.2014.11.030>
  33. Gonzalez-Torre I, Calzada-Perez MA, Vega-Zamánillo A, Castro-Fresno D (2015) Experimental study of the behaviour of different geosynthetics as anti-reflective cracking systems using a combined-load fatigue test. *Geotext Geomembranes* 43:345–350. <https://doi.org/10.1016/j.geotextmem.2015.04.001>
  34. Polidora J, Sobhan K, Reddy D V. (2019) Effects of geosynthetic inclusions on the fatigue and fracture properties of asphalt overlays. In: 17th European conference on soil mechanics and geotechnical engineering, ECSMGE-2019
  35. Nguyen ML, Chazallon C, Sahli M, et al (2020) Design of reinforced pavements with glass fiber grids: from laboratory evaluation of the fatigue life to accelerated full-scale test. In: accelerated pavement testing to transport infrastructure innovation. pp 329–338
  36. Pouteau B, Martin A, Berrada K, et al (2022) Impact of the performance of the asphalt concrete and the geogrid materials on the fatigue of geogrid-reinforced asphalt concrete—experimental study. In: Di Benedetto H, Baaj H, Chailleux E, et al (eds) RILEM International Symposium on Bituminous Materials. Springer: London. pp 1015–1021
  37. Canestrari F, Belogi L, Ferrotti G, Graziani A (2015) Shear and flexural characterization of grid-reinforced asphalt pavements and relation with field distress evolution. *Mater Struct Constr* 48:959–975. <https://doi.org/10.1617/s11527-013-0207-1>
  38. Virgili A, Canestrari F, Grilli A, Santagata FA (2009) Repeated load test on bituminous systems reinforced by geosynthetics. *Geotext Geomembranes* 27:187–195. <https://doi.org/10.1016/j.geotextmem.2008.11.004>
  39. Ghafoori N, Sharbat M (2016) Use of geogrid for strengthening and reducing the roadway structural sections
  40. Kim YR, Lee HJ, Little DN (1997) Fatigue characterization of asphalt concrete using viscoelasticity and continuum damage theory. In: journal of the association of asphalt paving technologists, volume 66. Salt Lake City, Utah, pp 520–569
  41. Rowe GM (1993) Performance of asphalt mixtures in the trapezoidal fatigue test. In: proceedings of the association of asphalt paving technologist, Volume 62. Austin, Texas, pp 344–384
  42. Reese RA (1997) Properties of aged asphalt binder related to asphalt concrete fatigue life. In: Journal of the Association of Asphalt Paving Technologists. Salt Lake City, Utah, pp 604–632
  43. Ghuzlan KA, Carpenter SH (2000) Criterion for fatigue testing. *Transp Res Rec J Transp Res Board*
  44. Hopman PC, Kunst PAJC, Pronk AC (1989) Renewed interpretation method for fatigue measurement, verification of miner's rule. In: proceedings of 4th eurobitumen symposium. Madrid, Spain, pp 557–561
  45. Pronk AC, Hopman PC (1991) Energy dissipation: the leading factor of fatigue. In: Highway research: sharing the benefits. pp 255–267
  46. Di Benedetto H, De La Roche C, Baaj H et al (2004) Fatigue of bituminous mixtures. *Mater Struct* 37:202–216. <https://doi.org/10.1007/bf02481620>
  47. Orešković M, Trifunović S, Mladenović G, Bohuš Š (2019) Fatigue resistance of a grid-reinforced asphalt concrete using four-point bending beam test. In: Nikolaides AF, Manthos E (eds) Bituminous mixtures and pavements VII. CRC Press, Thessaloniki, Greece, pp 589–594
  48. Van Dijk W, Visser W (1977) The energy approach to fatigue for pavement design. In: proceedings of the association of asphalt paving technologist. San Antonio, Texas, pp 1–40
  49. Di Benedetto H, Nguyen QT, Sauzéat C (2011) Non-linearity, heating, fatigue and thixotropy during cyclic loading of asphalt mixtures. *Road Mater Pavement Des* 12:129–158. <https://doi.org/10.1080/14680629.2011.9690356>
  50. Pérez-Jiménez F, Botella R, Miró R (2012) Damage and thixotropy in asphalt mixture and binder fatigue tests. *Transp Res Rec* 31:8–17. <https://doi.org/10.3141/2293-02>
  51. Blakenship P, Rowe GM (2019) Fatigue assessment of conventional and highly modified asphalt materials with ASTM and AASHTO Specifications. In: 12th conference on asphalt pavements for Southern Africa. Sun City, South Africa
  52. Shen S, Lu X (2011) Energy based laboratory fatigue failure criteria for asphalt materials. *J Test Eval* 39:313–320. <https://doi.org/10.1520/JTE103088>
  53. Abojaradeh MA, Witczak MW, Mamlouk MS, Kaloush KE (2007) Validation of initial and failure stiffness definitions in flexure fatigue test for hot mix asphalt. *J Test Eval* 35:95–102. <https://doi.org/10.1520/jte100102>
  54. Hopman PC, Kunst P, Pronk AC (1989) A renewed interpretation method for fatigue measurements - verification of Miner's Rule. In: Proceedings of The 4th Eurobitume Symposium, Madrid. Madrid, Spain, pp 557–561
  55. Li X, Youtcheff J (2018) Practical method to determine the effect of air voids on the dynamic modulus of



- asphalt mixture. *Transp Res Rec* 2672:462–470. <https://doi.org/10.1177/0361198118787389>
56. Santagata FA, Partl MN, Ferrotti G, et al (2008) Layer characteristics affecting interlayer shear resistance in flexible pavements. In: *journal of the association of asphalt paving technologists. association of asphalt paving technologists (AAPT)*, pp 221–256
  57. Zhou F, Fernando E, Scullion T (2009) Transfer functions for various distress types (Report No. FHWA/TX-08/0–5798-P2)
  58. Bohus S, Sperka P, Kudrna J (2023) Investigations on shear bond characteristics of grid reinforced asphalt concrete. In: *XXVIIth World Road Congress. PIARC -World Road Association, Prague, Czech Republic*

**Publisher's Note** Springer Nature remains neutral with regard to jurisdictional claims in published maps and institutional affiliations.

